Supporting Information

Levitan et al. 10.1073/pnas.1419818112

SI Materials and Methods

Cultivation and Experimental Planning. *Phaeodactylum tricornutum* (accession Pt1 8.6, the Provasoli–Guillard National Center for Culture of Marine Phytoplankton) was maintained axenically in sterile artificial seawater enriched with F/2 nutrients (1, 2). A set of three optically thin, biologically independent cultures was maintained under exponential growth conditions starting at 2.5×10^5 cells/mL in UltraCruz flasks at 18 °C and 120–150 μmol photons $m^{-2}s^{-1}$ continuous white light emitting diodes (LEDs) and aerated through 0.2-μm filters. Cell densities were determined using a Beckman Coulter Multisizer 3 (Beckman Coulter Inc.). After 48 h of growth, cells were centrifuged, washed two times with nitrogen-free, artificial seawater-based F/2, and split into nitrogen-replete and -free conditions. To assure the largest contrast between the physiological states, both treatments were sampled after 48 h. Cultures were sampled while the N-replete culture was in exponential growth and the N-stressed culture ceased dividing for 24 h; however, both cultures were still optically thin. Cultures of the KD strain, NR21, were maintained under the same conditions as the WT and supplemented with 100 μg/mL Zeocin (R-250; Invitrogen).

Lipid Analyses. Lipids were extracted from $\sim 5 \times 10^7$ cells filtered onto Whatman glass fiber filters (GF/F) using a modified Bligh and Dyer (3) protocol as described previously (4). IPL analysis was performed using HPLC/electrospray ionization MS (4) on an Agilent 1200 HPLC and Thermo TSQ Vantage Ion Trap MS. Total extracts were analyzed for TAGs by nonaqueous reverse-phase HPLC/atmospheric pressure chemical ionization MS (5) on an Agilent 1200 HPLC and Agilent 1200 Single-Quadrapole MS. We identified distinct TAGs by their mass spectra using the protocol described by Holčapek et al. (5, 6). For analysis of cellular lipids in the WT and NR21 strain, we measured the amount of FAMEs in exponentially growing cultures as previously described (7–9).

Protein Analysis. For determination of the amounts of protein subunits, cultures were spun down at 4 °C and frozen in liquid N_2. Samples were resuspended in 1× denaturating lithium dodecyl sulfate extraction buffer, and proteins were extracted by sonication (Qsonica). Total protein concentration was measured using a modified Lowry assay (DC 500–0111; Bio-Rad) and a SpectraMax M3microplate reader (Molecular Devices) at 750 nm. BSA served as the comparative protein standard.

Abundance of four independent protein subunits was detected by Western blotting. For anti-NR and anti-DGAT2D, we used our own custom-made anti-rabbit antibodies (Thermo Scientific and Pierce Antibody Products) at 1:500–1:1,000 dilution. For the photosynthetic subunits, we used Agrisera antibodies, anti-PsbA (AS01 016), and anti-RbcL (AS03 037) at 1:10,000 dilution. HRP-conjugated goat anti-rabbit IgG HRP secondary antibody (A6154; Sigma-Aldrich) was used as a secondary antibody for all samples; 1–10 μg total protein was separated electrophoretically on precast 4–20% Tris-glycine extended (TGX) gels (Bio-Rad), and proteins were transferred to PVDF membranes using a Trans-Blot Turbo Dry Transfer System and Transblot Turbo PVDF Transfer Packs (Bio-Rad). Blots were developed with Amersham ECL Select Detection Reagent (RPN2235; GE Healthcare). The blots were quantified using a ChemiDoc MP Imaging System (Bio-Rad) and the Image Lab software (Bio-Rad).

Quantification of NR mRNA Copies—Real-Time Quantitative PCR. Samples for quantitative PCR (qPCR) were pelleted by centrifuging 5×10^7 cells for 8 min at 6,000 × *g* using a Sorvall RC6+ Centrifuge (Thermo Scientific) at 4 °C. The samples were frozen in liquid N_2 and stored at −80 °C. Total RNA was extracted using an RNAeasy Plant Mini Kit (Qiagen) followed by removal of DNA contamination using Ambion Turbo DNase (AM1907; Life Technologies). PCR was performed to confirm that there was no DNA contamination. Total RNA quantification and quality assessment were made spectrophotometrically with a Nanodrop 1000 (Thermo Scientific). cDNA was generated using oligodT as primers and a SuperScript III Kit (12574-026; Life Technologies) and directly used as the template for qPCR. Primers for NR gene were designed with National Center for Biotechnology Information Primer-BLAST (www.ncbi.nlm.nih.gov/tools/primer-blast/). qPCR was performed using the Applied Biosystems SYBR Green PCR Master Mix (4309155; Life Technologies) on a Mx3000P QPCR System (Agilent Technologies). Standard plasmids with the NR sequence were generated by cloning the NR amplicon onto a TOPO TA Vector (Life Technologies). A serial dilution of the plasmid as the standard curve (five orders of magnitude) was run together with the unknown biological samples for copy number calculation (8). All standard curves had an $r^2 > 0.94$. The qPCR amplification of the samples was compared with the calibration curve to calculate the gene copy number present.

NR Activity Assay. NR activity was measured following the method described by Eppley (10) with modifications (11). Triplicates samples (5×10^6 cells) of exponentially growing WT and NR21 cultures were harvested on a 25-mm glass fiber filter (GF/F) and homogenized in 1 mL ice-cold extraction buffer [200 mM phosphate buffer, pH 7.9, 1 mM DTT, 0.3 (wt/vol) polyvinyl pyrrolidone, 3% (wt/vol) BSA, 0.1% Triton, 5 mM EDTA] using a glass Teflon homogenizer. The slurries were centrifuged at 4,300 × *g* for 5 min at 4 °C, and the supernatant was removed and used immediately for the assay. Assays were conducted in a total volume of 1 mL containing final concentrations of 200 mM phosphate buffer (pH 7.9) and 2.5 μM NADH in 200 μL supernatant. To begin the assay, KNO_3 was added at a final concentration of 10 μM, and samples were incubated at 20 °C for 45 min. The reaction was stopped by adding 2 mL zinc acetate solution to a final concentration of 0.18 M. The solution was centrifuged shortly, and the supernatant was transferred to clean Eppendorf tubes; 100 μL color developer (sulfanilamide, *N*-(1 naphtyl)-ethylenediamine.2HCl) was added, and samples were incubated for 30 min at room temperature before reading their absorbance at 543 nm. The activity was calculated against a standard curve as units per cell, where one unit of enzyme activity catalyzes the conversion of 1 μmol substrate to product per minute.

Analysis of RNA-Seq Data. After aligning the raw data to *P. tricornutum*'s version 2.0 set 10,402 filtered gene models (genome.jgi.doe.gov/Phatr2/Phatr2.info.html), files were filtered to retrieve uniquely aligned reads with no more than three mismatches. Gene counts (unique aligned reads per gene) were used for DE analysis carried out using the DESeq R/Bioconductor package (12), which infers DE based on the negative binomial distribution. For this analysis, we used a cutoff of 5% to control for false detection rate (false positives) and considered only genes that had a log twofold change greater than or equal to ±2

and a false detection rate < 0.05 to be DE. To define the changes in biochemically important pathways and/or physiological function, we set 16 gene categories (Dataset S1) that represent major biochemical and regulatory functions. To establish the pathway boundaries, we assigned genes using the Diatomcyc (www.diatomcyc.org/) guidelines and the KEGG database (13) and manually using publications inserted into the databases (14, 15). DESeq's output for all 10,402 genes was submitted to the Gene Expression Omnibus under accession no. GSE56346, and all reads were deposited to the National Center for Biotechnology Information's Short Read Archive under accession no. SRP040703.

Calculation and Analysis of the Computational Metabolic Flux Prediction. To calculate this correlation, we used the uncentered Pearson product–moment correlation, which is a popular measure of the linear correlation between two variables:

$$\max \frac{v_{\text{irr}} \cdot g_{\text{irr}}}{\|v_{\text{irr}}\| \|g_{\text{irr}}\|}$$

$$\text{subject to} \begin{cases} Sv = 0 \\ a_j \le v_j \le b_j \end{cases},$$

where v_{irr} is a flux vector representing the reaction rates of the irreversible reactions in the network, and g_{irr} is a vector indicating corresponding gene expression data. We used the set of irreversible reactions when maximizing the correlation, because the directions of reversible reactions are undefined, whereas gene expression data values are always positive. The predicted fluxes were normalized by growth rates measured under the N-replete and N-depleted conditions (8, 9). The metabolic fluxes layout was generated by Cytoscape v.2.8.3 (16).

Constructing the NR Inverted Repeat Vector. For constructing the inverted repeat part of the vector, we chose to focus on the NADH binding domain at the C terminus of the sequence (17). We amplified 250- and 400-bp fragments corresponding to NR gene sequence from 2,338 to 2,587 bp and from 2,338 to 2,737 bp by PCR using the primers with EcoRI and XbaI restriction sites (underlined). The primers sequences (5′ to 3′) were NR-F: CCCGAATTCGTTTTACAATCGACGCCG; NR-R1: CCCTCTAGAGAAGACCCAGCTGTCA; and NR-R2: CCCTCTAGATTGTGACCAAGGCTC. The two fragments shared the first 250 bp. Both long and short fragments were amplified and digested by EcoRI and XbaI and ligated into an EcoRI-linearized pKS-*Sh ble*-FA vector to form a sense and an antisense hairpin based on the XbaI site of the two amplicons to make a pKS-*Sh ble nr*IR-FA vector. The vector was propagated using heat shock transformation of One Shot TOP10 Chemically Competent *Escherichia coli* (C4040-10; Invitrogen) and purified using the QIAprep Spin Miniprep Kit (27104; Qiagen). To verify the sequence of the fragment that was inserted to the plasmid, the purified plasmids were submitted for sequencing (Genewiz Inc.).

Genetic Transformation and Screening for Transformants. Five micrograms pKS-*Sh ble nr*IR-FA vector was coated onto M17 tungsten particles (1.1 μm) according to the manufacturer's instructions (Bio-Rad). Approximately 5×10^7 *P. tricornutum* cells were plated on 1% agar plates (50% F/2) and incubated for several hours before the transformation. The cells were bombarded with the DNA-coated M17 at 1,550 psi using a PDS-1000/He Particle Delivery System (Bio-Rad) as previously described (18). The plates were incubated at 100 μmol photons m^2 s^{-1} constant illumination at 18 °C for 48 h to recover. Cells were then replated onto selective 1% agar plates (50% F/2) with 880 μM NH_4Cl as the sole nitrogen source and 50 μg/mL phleomycin (ant-ph; Invitrogen). Plates were incubated at 40 μmol photons m^2 s^{-1} for 1 mo to enable putative silent clones to grow. The insertion of the introduced DNA into the strain was verified by PCR of the antibiotic-resistant gene.

Three independent transformations with our plasmid yielded 170 colonies. To select for the best clone, cells were grown in liquid f/2, starved for nitrogen (48 h), and then incubated in fresh media (culture concentration – 2×10^5 cells/mL) with 880 μM $NaNO_3$ as the sole nitrogen source. Each culture was then split into two cultures. One was treated with a final concentration of 17 mM chlorate ($ClKO_3$), and the other served as a control. Based on the ability of the NR to reduce chlorate to toxic chlorite ion (ClO_2^-) (19), cells that exhibited the highest survival rates 5 d after the addition of the chlorate were chosen for additional analysis. Of 170 colonies, six strains were analyzed for their growth rates, PSII photosynthetic yields, FAMEs, C and N content, TAG amount, and NR activity under nitrogen-replete exponential growth (data not shown). The strain that exhibited ~50% NR activity and 20% increase in FAMEs amount (NR21) was chosen for additional studies.

1. Goldman JC, McCarthy JJ (1978) Steady state growth and ammonium uptake of a fast-growing marine diatom. *Limnol Oceanogr* 23(4):695–703.
2. Guillard RR, Ryther JH (1962) Studies of marine planktonic diatoms. I. Cyclotella nana Hustedt, and Detonula confervacea (cleve) Gran. *Can J Microbiol* 8(2):229–239.
3. Bligh EG, Dyer WJ (1959) A rapid method of total lipid extraction and purification. *Can J Biochem Physiol* 37(8):911–917.
4. Popendorf KJ, Fredricks HF, Van Mooy BA (2013) Molecular ion-independent quantification of polar glycerolipid classes in marine plankton using triple quadrupole MS. *Lipids* 48(2):185–195.
5. Holčapek M, Lísa M, Jandera P, Kabátová N (2005) Quantitation of triacylglycerols in plant oils using HPLC with APCI-MS, evaporative light-scattering, and UV detection. *J Sep Sci* 28(12):1315–1333.
6. Holčapek M, Jandera P, Zderadička P, Hrubá L (2003) Characterization of triacylglycerol and diacylglycerol composition of plant oils using high-performance liquid chromatography-atmospheric pressure chemical ionization mass spectrometry. *J Chromatogr A* 1010(2):195–215.
7. Rodríguez-Ruiz J, Belarbi E-H, Sánchez JLG, Alonso DL (1998) Rapid simultaneous lipid extraction and transesterification for fatty acid analyses. *Biotechnology Techniques* 12(9):689–691.
8. Guerra LT, et al. (2013) Regulatory branch points affecting protein and lipid biosynthesis in the diatom *Phaeodactylum tricornutum*. *Biomass Bioenergy* 59:306–315.
9. Frada MJ, Burrows EH, Wyman KD, Falkowski PG (2013) Quantum requirements for growth and fatty acid biosynthesis in the marine diatom *Phaeodactylum tricornutum* (Bacillariophyceae) in nitrogen replete and limited conditions. *J Phycol* 49(2):381–388.
10. Eppley RW, Rogers JN, McCarthy JJ, Sournia A (1971) Light/dark periodicity in nitrogen assimilation of the marine phytoplankters *Skeletonema costatum* and coccolithus huxleyi in n-limited chemostat culture. *J Phycol* 7(2):150–154.
11. Berges JA, Harrison PJ (1995) Nitrate reductase-activity quantitatively predicts the rate of nitrate incorporation under steady-state light limitation—a revised assay and characterization of the enzyme in three species of marine-phytoplankton. *Limnol Oceanogr* 40(1):82–93.
12. Anders S, Huber W (2010) Differential expression analysis for sequence count data. *Genome Biol* 11(10):R106.
13. Kanehisa M, Goto S, Sato Y, Furumichi M, Tanabe M (2012) KEGG for integration and interpretation of large-scale molecular data sets. *Nucleic Acids Res* 40(Database issue D1):D109–D114.
14. De Martino A, et al. (2011) Physiological and molecular evidence that environmental changes elicit morphological interconversion in the model diatom *Phaeodactylum tricornutum*. *Protist* 162(3):462–481.
15. Rayko E, Maumus F, Maheswari U, Jabbari K, Bowler C (2010) Transcription factor families inferred from genome sequences of photosynthetic stramenopiles. *New Phytol* 188(1):52–66.
16. Smoot ME, Ono K, Ruscheinski J, Wang P-L, Ideker T (2011) Cytoscape 2.8: New features for data integration and network visualization. *Bioinformatics* 27(3):431–432.
17. Allen AE, Ward BB, Song B (2005) Characterization of diatom (bacillariophyceae) nitrate reductase genes and their detection in marine phytoplankton communities. *J Phycol* 41(1):95–104.
18. Falciatore A, Casotti R, Leblanc C, Abrescia C, Bowler C (1999) Transformation of nonselectable reporter genes in marine diatoms. *Mar Biotechnol (NY)* 1(3):239–251.
19. Solomonson LP, Vennesland B (1972) Nitrate reductase and chlorate toxicity in Chlorella vulgaris Beijerinck. *Plant Physiol* 50(4):421–424.

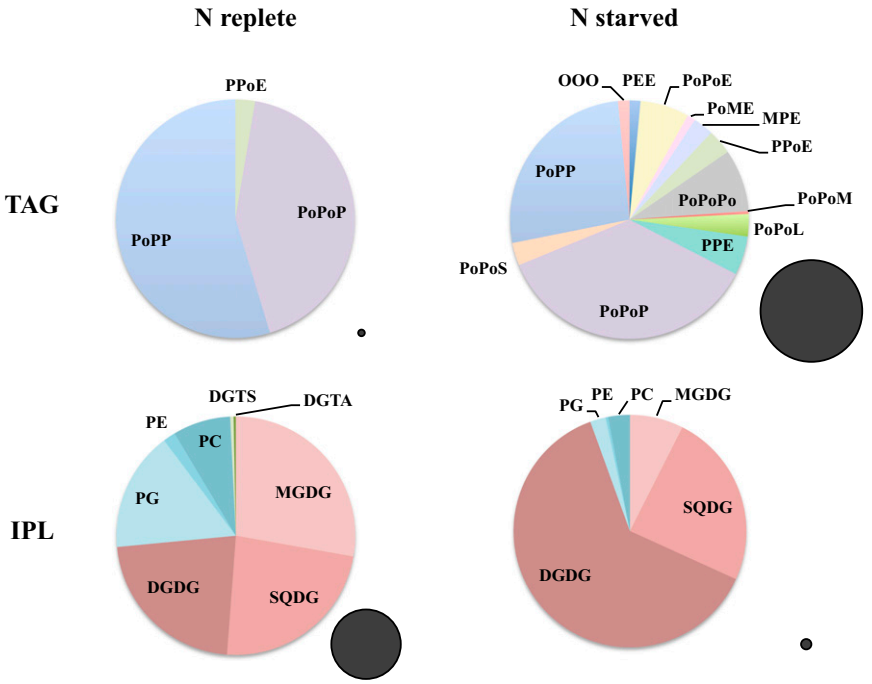

Fig. S1. Distribution and relative abundance of specific TAGs and IPLs in *P. tricornutum* grown under nitrogen-stressed and -replete conditions. Data are presented as percentage of the carbon in a specific lipid from the total amount of carbons allocated to either TAG or IPL. Dark gray circles represent the percentages of the cellular carbon allocated to total TAGs and IPLs for each condition.

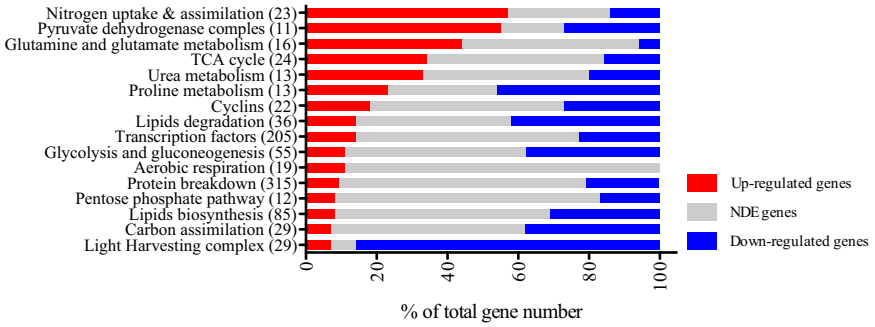

Fig. S2. Transcripts abundance (nitrogen-stressed/nitrogen-replete) of genes from 16 gene families that are central to *P. tricornutum* metabolic and regulatory pathways. Changes are denoted as the percentage of up-regulated (red), NDE (gray), and down-regulated genes (blue) within each gene family. The full description of the gene families and assigned genes with their fold change, false detection rate (FDR), and description can be found in Dataset S1.

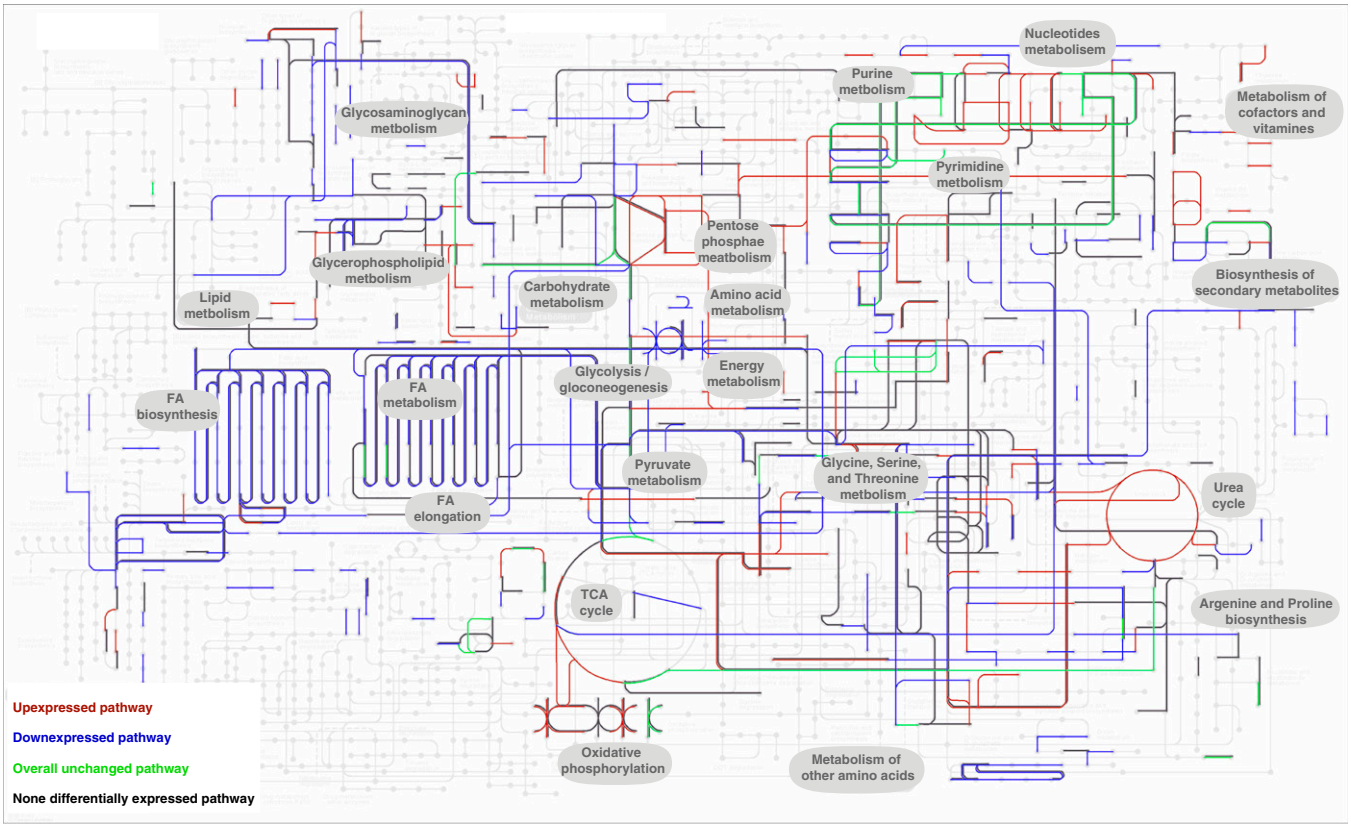

Fig. S3. Representation of the DE pattern of metabolic pathways in *P. tricornutum* grown under nitrogen-stressed to nitrogen-replete conditions shown on the KEGG metabolic pathway. The red lines represent pathways that were overall up-regulated, the blue lines represent pathways that were overall down-regulated (more than 50% of the genes), the green lines represent pathways that were not up- or down-regulated, and the black lines represent genes in pathways that were NDE.

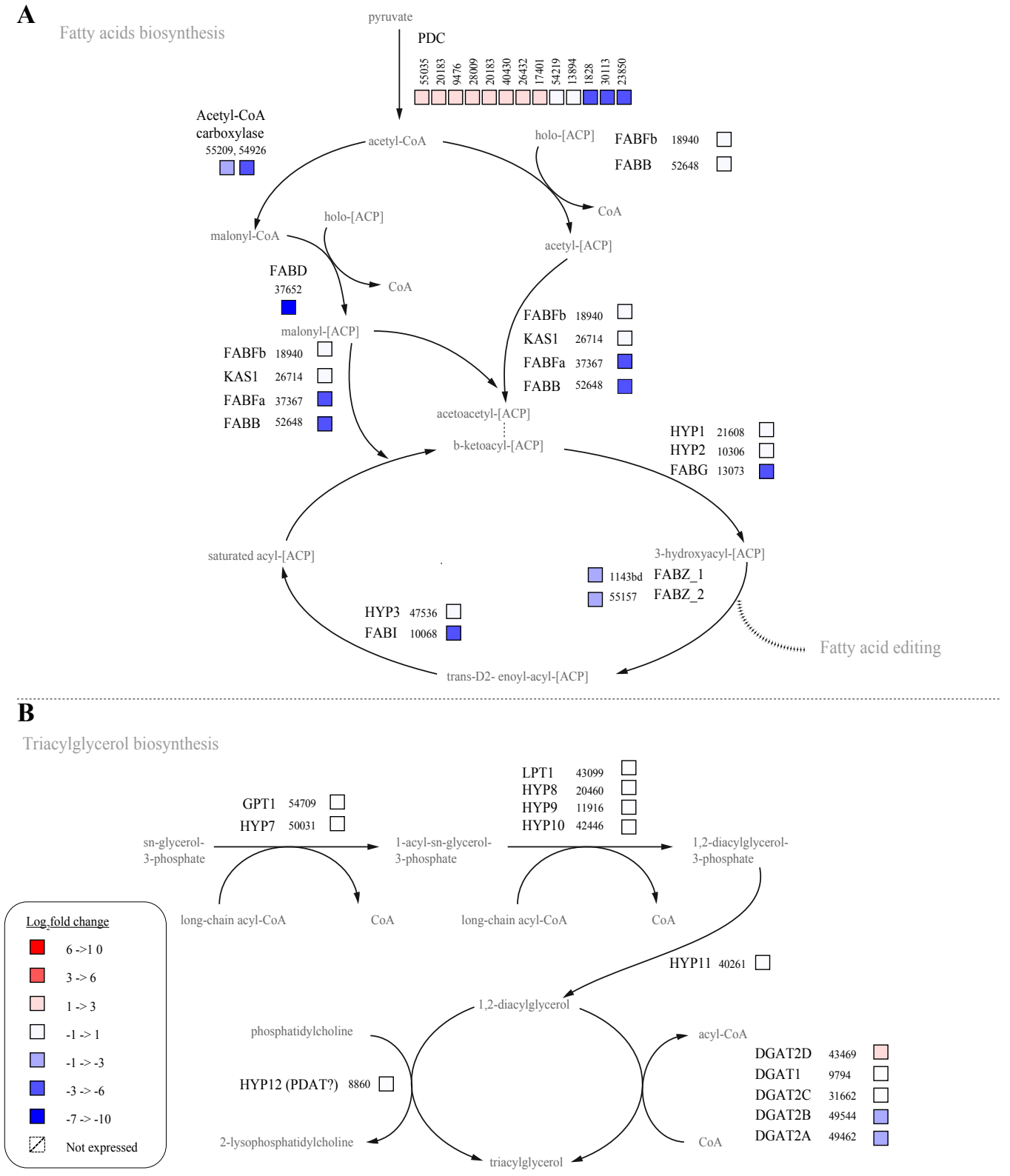

Fig. S4. Changes in the transcript abundance (nitrogen-stressed/nitrogen-replete) of genes involved in *P. tricornutum*'s lipid biosynthesis. (*A*) FAs biosynthesis. (*B*) TAG biosynthesis. The genes are noted with gene numbers and names. The full description of the genes, exact fold-change values, and false detection rate can be found in Dataset S1. ACP, acyl carrier protein; FABD, malonyl-CoA:ACP transacylase; FABF and FABB, 3-oxoacyl-[acyl-carrier-protein] synthase; FABZ, 3R-hydroxyacyl-[acyl carrier protein] dehydrase; GPT1, glycerol-3-phosphate o-acyltransferase; HYP, hypothetical protein; KAS1 and FABG, beta ketoacyl-coa synthase; LPT1, 1-acyl-sn-glycerol-3-phosphate acyltransferase; PDC, pyruvate dehydrogenase complex; PDAT, phospholipid:diacylglycerol acyltransferase.

Table S1. Lipid analysis for *P. tricornutum* grown under N-replete and N-starved conditions: IPL

IPL	N-replete		N-starved		Ratio (N-starved to N-replete)
	Fmol/cell	Cellular C (%)	Fmol/cell	Cellular C (%)	
Specific IPL amount					
Total	2.43 ± 0.15	8.4	0.87 ± 0.13	2.5	0.36
MGDG	0.47 ± 0.61	2.3	0.06 ± 0.01	0.2	0.13
DGDG	0.67 ± 0.09	2.0	0.21 ± 0.03	0.6	0.32
SQDG	0.63 ± 0.19	1.9	0.54 ± 0.08	1.6	0.85
PG	0.49 ± 0.06	1.4	0.02 ± 0.01	0.1	0.04
PE	0.05 ± 0.00	0.1	0.00 ± 0.00	0.0	0.07
PC	0.26 ± 0.09	0.7	0.03 ± 0.01	0.1	0.12
DGTS	0.01 ± 0.00	0.0	0.00 ± 0.00	0.0	—
DGTA	0.01 ± 0.00	0.0	0.00 ± 0.00	0.0	—
Molar ratios (%)					
Galactolipids/IPL	32 ± 1.0		6 ± 1.0		0.19
Phospholipids/IPL	39 ± 0.5		69 ± 0.5		1.77
SQDG/IPL	28 ± 0.6		24 ± 0.6		0.89
Betain lipids/IPL	0.8 ± 0.0		0.0 ± 0		—
Ratios between lipids classes					
IPL/TAG	12 ± 2.4		0.5 ± 0.17		
SQDG/PG	1.4 ± 0.0		11.3 ± 2.7		
PE/PC	0.2 ± 0.0		0.1 ± 0.0		

Data are presented in femtomoles per cell and percentage of the carbons allocated to the specific lipid or total lipid subclass (IPL or TAG) from the total cellular carbon. DGDG, digalactosyldiacylglycerol; DGTA, diacylglyceryl hydroxymethyltrimethyl-β-alanine; DGTS, diacylglyceryltrimethylhomoserine; MGDG, monogalactosyldiacylglycerol; PC, phosphatidylcholine; PE, phosphatidylethanolamine; PG, glycerophosphoglycerols; SQDG, sulfoquinovosyldiacylglycerol.

Table S2. Lipid analysis for *P. tricornutum* grown under N-replete and N-starved conditions: TAG

TAG	N-replete		N-starved		Ratio (N-starved to N-replete)
	Fmol/cell	Cellular C (%)	Fmol/cell	Cellular C (%)	
Specific TAG amount					
Total	0.21 ± 0.05	0.8	1.9 ± 0.11	12.3	8.9
PEE (16:0, 20:5, 20:5)	0.00 ± 0.00	0.0	0.02 ± 0.00	0.2	—
PoPoE (16:1, 16:1, 20:5)	0.00 ± 0.00	0.0	0.13 ± 0.02	0.8	—
PoME (16:1, 14:0, 20:5)	0.00 ± 0.00	0.0	0.02 ± 0.02	0.1	—
MOLn (14:0, 18:1, 18:3)	0.00 ± 0.00	0.0	0.00 ± 0.00	0.0	—
MPE (14:0, 16:0, 20:5)	0.00 ± 0.00	0.0	0.05 ± 0.02	0.3	—
PPoE (16:0, 16:1, 20:5)	0.02 ± 0.00	0.0	0.06 ± 0.01	0.4	3.72
PoPoPo (16:1, 16:1, 16:1)	0.00 ± 0.00	0.0	0.16 ± 0.04	1.0	—
PoPoM (16:1, 16:1, 14:0)	0.00 ± 0.00	0.0	0.01 ± 0.01	0.0	—
PoPoL (16:1, 16:1, 18:2)	0.00 ± 0.00	0.0	0.06 ± 0.03	0.4	—
PPE (16:0, 16:0, 20:5)	0.00 ± 0.00	0.0	0.09 ± 0.03	0.7	—
PoPoP (16:1, 16:1, 16:0)	0.09 ± 0.01	0.3	0.68 ± 0.19	4.5	7.48
PoPoS (16:1, 16:1, 18:0)	0.00 ± 0.00	0.0	0.06 ± 0.02	0.4	—
PoPP (16:1, 16:0, 16:0)	0.12 ± 0.04	0.4	0.50 ± 0.19	3.3	4.29
OOO (18:1, 18:1, 18:1)	0.00 ± 0.00	0.0	0.03 ± 0.02	0.2	—
Specific FA from total TAG (%)					
14:0	0		1		—
16:0	52		36		0.69
16:1	47		52		1.69
18:0	0		1		—
18:1	0		1		—
18:2	0		1		—
18:3	0		0		—
20:5	1		8		8.40

Data are presented in femtomoles per cell and percentage of the carbons allocated to the specific lipid or total lipid subclass (IPL or TAG) from the total cellular carbon. The different TAGs are denoted according to their FAs content. The different FAs are marked as follows: M, 14:0; P, 16:0; Po, 16:1; S, 18:0; O, 18:1; L, 18:2; E, 20:5.

Table S3. Calculation of the cellular fluxes of reductant directed to photosynthetic carbon fixation and nitrate reduction in the WT and nitrogen-starved *P. tricornutum* and the NR21 strain: The allocation reductant between carbon fixation and nitrate reduction

Strain, condition	μ (d^{-1})	Cellular C (mol/cell)	Cellular N (mol/cell)	C:N (mol:mol)	CO_2:O_2	Cellular reductant to C fixation (%)	Cellular reductant to nitrate (%)
WT, N-replete	0.80	1.5×10^{-12}	2.5×10^{-13}	5.70	0.74	74	26
WT, N-starved	0.30	7.8×10^{-13}	4.68×10^{-14}	17.08	0.90	90	10
NR21, N-replete	0.53	1.9×10^{-12}	2.7×10^{-13}	7.16	0.78	78	22

Table S4. Calculation of the cellular fluxes of reductant directed to photosynthetic carbon fixation and nitrate reduction in the WT and nitrogen-starved *P. tricornutum* and the NR21 strain: Calculated daily cellular NADPH flux

Strain, condition	Photosynthetic quotient	Flux of photosynthetically fixed C (mol/d)	O_2 flux (mol/d)	Electron flux (mol/d)	NADPH flux (mol/d)
WT, N-replete	1.35	1.16×10^{-12}	1.57×10^{-12}	6.27×10^{-12}	3.13×10^{-12}
WT, N-starved	1.12	2.34×10^{-13}	2.62×10^{-13}	1.05×10^{-12}	5.23×10^{-13}
NR21, N-replete	1.28	1.01×10^{-12}	1.30×10^{-12}	5.19×10^{-12}	2.59×10^{-12}

Table S5. Calculation of the cellular fluxes of reductant directed to photosynthetic carbon fixation and nitrate reduction in the WT and nitrogen-starved *P. tricornutum* and the NR21 strain: Fraction of NADPH required for the reduction of carbon into FAMEs

Strain, condition	Cellular C allocated to FAMEs* (%)	C in FAMEs (mol/cell)	Flux of C to FAMEs (mol/d)	NADPH flux in FAME synthesis (%)
WT, N-replete	0.14	2.00×10^{-13}	1.60×10^{-13}	5
WT, N-starved	0.28	2.20×10^{-13}	6.60×10^{-14}	13
NR21, N-replete	0.21	4.00×10^{-13}	2.10×10^{-13}	8

Calculations are based on experimental results (C per cell, N per cell, μ, and FAMEs per cell) and a steady-state growth model adapted from Falkowski et al. (1).
*Data are from Fig. 1.

1. Falkowski PG, Dubinsky Z, Wyman K (1985) Growth-irradiance relationships in phytoplankton. *Limnol Oceanogr* 30(2):311–321.

Dataset S1. A summary of all of the genes assigned to 16 gene categories, including their log_2 fold change, false detection rate, and metabolic description

Dataset S1

Metabolic descriptions were added after our bioinformatics analysis that include information given in Diatomcyc and JGI databases and the *P. tricornutum* Digital Gene Expression Database.